PCCP

PAPER

View Article Online
View Journal | View Issue

Cite this: *Phys. Chem. Chem. Phys.*, 2019, **21**, 4184

Three-dimensionally patterned Ag–Pt alloy catalyst on planar Si photocathodes for photoelectrochemical H_2 evolution†

Sung Yul Lim, ‡[a] Kyungyeon Ha,‡[bc] Heonhak Ha, ‡[d] Soo Youn Lee, [a] Min Seok Jang, *[d] Mansoo Choi *[bc] and Taek Dong Chung *[ae]

Received 28th November 2018,
Accepted 23rd January 2019

DOI: 10.1039/c8cp07304j

rsc.li/pccp

Platinum is still the most active element for the hydrogen evolution reaction (HER); however, it suffers from its scarcity and high cost. Thus, significant efforts have been dedicated to maximize the catalytic activity with less loading. When Pt is utilized at a semiconductor surface, more factors have to be considered. Placing a catalyst directly in contact with a semiconductor supports the extraction of photogenerated minority carriers as well as boosts the catalytic reactions. In addition, a catalyst should be designed with prudence not to interfere in the light path with respect to absorption at the underlying substrate. Herein, we report the development of planar Si-based photocathodes, covered with a native oxide, for the HER, which also satisfy the prerequisites for the use of a three-dimensionally patterned, flower-like Ag–Pt catalyst. The catalyst consisted of nanoparticles of homogeneously alloyed Ag and Pt, fabricated by a galvanic exchange of Pt with Ag. Importantly, these two elements were proven to have their own functionalities. Ag not only contributed to transporting e^- and H_{ad} to the Pt for subsequent processes of the HER but also effectively extracted minority carriers by diluting the high work function of Pt, leading to a better Schottky barrier at the catalyst–insulator–semiconductor junction. Furthermore, computational simulation revealed that the proposed catalyst pattern alleviated optical light loss with the increasing catalyst loading compared to the two-dimensional case. Owing to these effects, we could achieve 0.36 V (*vs.* reversible hydrogen electrode) as an open circuit potential and the near maximum current density of planar p-type Si. The findings in this work suggests deeper insights that could support the design of catalysts for solar-fuel systems.

Introduction

With an aim to mimic the photosynthesis in nature, numerous research works have focused on the conversion of intermittent solar power into a storable form of energy, such as by chemical bonding, to meet the increasing energy demands of human society.[1,2] Hydrogen (H_2), obtained by splitting water molecules ($H_2O \rightarrow H_2 + 1/2\ O_2$), is a promising solar fuel, owing to its zero-emission nature and higher energy density (120 MJ kg^{-1}) than methane (50 MJ kg^{-1}) and gasoline (43 MJ kg^{-1}).[3,4] Several device designs have been proposed for solar-driven water-splitting, *e.g.*, photocatalyst colloids, photovoltaic modules connected to electrolyzers, and photoelectrochemical cells (PECs).[5] Among these, PECs involve an intriguing approach because of their technological maturity and low manufacturing cost. A typical PEC consists of at least three components: membranes or other similar architectures, preventing product cross-over between the cathode and anode; light absorbers to generate excitons for generating photovoltage; and catalysts to facilitate the (photo)electrochemical reactions.[6]

It is believed that the overall PEC performance of the catalyst component is significantly dependent on the distribution of the catalysts,[7,8] the interface with the underlying semiconductor junction,[9] and the light absorption efficiency,[10] even for the same material. First, meticulous care is imperative to prevent substantial photon loss by scattering and reflection at the catalyst layer. The trade-off between the activity and optical obscuration of an electrocatalyst can be adjusted by leaving the

[a] *Department of Chemistry, Seoul National University, Seoul 08826, Korea. E-mail: tdchung@snu.ac.kr*
[b] *Department of Mechanical and Aerospace Engineering, Seoul National University, Seoul 08826, Korea. E-mail: mchoi@snu.ac.kr*
[c] *Global Frontier Center for Multiscale Energy Systems, Seoul National University, Seoul 08826, Korea*
[d] *School of Electrical Engineering, Korea Advanced Institute Science and Technology (KAIST), Daejeon 34141, Korea. E-mail: jang.minseok@kaist.ac.kr*
[e] *Advanced Institutes of Convergence Technology (AICT), Suwon-Si, Gyeonggi-do 16229, Korea*

† Electronic supplementary information (ESI) available. See DOI: 10.1039/c8cp07304j

‡ These authors contributed equally to this work.

semiconductor surfaces bare for more efficient light transmission. Based on a report by Chen *et al.*,[7] a maximum solar-to-hydrogen conversion efficiency of 24.9%, which was close to the ideal value, could be acquired by using patterned Pt ultramicroelectrode arrays on a semiconductor electrode. A recent paper published by Oh *et al.* stated that micrometer-scale patterned NiFe with a three-dimensional (3D) inverse opal structure facilitated water oxidation on an n-type Si photoanode.[11] Engineering of the photoelectrode interface is also important to enhance facile electron transfer from light absorbers to molecules through the catalyst layer. Ji *et al.*,[12] Hu *et al.*,[13] and Seger *et al.*[14] showed that it is possible to achieve a near-maximum saturated photocurrent density (J_{SC}) of crystalline Si by replacing the Si-based tunneling barrier with $SrTiO_3$ or TiO_2, which facilitates electron tunneling through the conduction band of the oxide layer. Third, the PEC performance can be enhanced not only by incorporating a high-quality protection layer between the catalyst and semiconductor, but also by using a proper catalyst combination with the specific semiconductor surface to improve the junction property.[15] Esposito *et al.* reported that the introduction of a 30 nm thick Ti layer underneath Pt could induce a positive shift of the open circuit potential (V_{OC}) for HER at p-Si(100) photocathodes.[15] The Ti enables a greater extraction of photogenerated carriers from p-Si(100) and passes the charge carriers to the upper layer for facile electron transfer to molecules in the electrolyte.[15] These previous results unequivocally demonstrate that engineering catalyst/semiconductor junctions can remarkably influence the electron–hole separation efficiency, photovoltage, and electrocatalytic reactions.

Herein, we demonstrate an enhancement in light absorption and photovoltage using a three-dimensionally (3D) patterned Ag–Pt alloy catalyst on planar p-Si(100) photocathodes. The specially designed planar-type Si photocathode generated a V_{OC} of 0.36 V (*vs.* reversible hydrogen electrode (RHE)) and J_{SC} of -36 mA cm^{-2}. A galvanic exchange of pre-patterned Ag nanostructures with $[PtCl_4]^{2-}$ yielded the bimetallic Ag–Pt catalyst, retaining the original flower-like configuration. The horizontally patterned catalyst and the bare Si, that is covered by native oxide (SiO_x), surface open to the transparent electrolyte solution allowed for the efficient transmission of light to the underlying semiconductor, while the vertically grown Ag structure provided a substrate for a sufficient amount of Pt to promote Faradaic reactions. In addition, it was expected that Ag would effectively supply electrons and protons to Pt, which functioned as the reaction site for HER owing to its high intrinsic conductivity[16] and tendency for hydrogen atom adsorption (H_{ad}).[17] More importantly, Ag can improve the efficiency of photogenerated electrons extraction from semiconductor substrate compared to direct contact with pure Pt and p-Si. Ag is widely used to form a Schottky diode interface when it meets with p-Si owing to its low work function (4.26 eV, comparable with Ti).[18] Owing to this improved junction property, we achieve a V_{OC} of 0.36 V, which is about 100 mV higher than any other reported cases utilizing low-quality SiO_x-covered planar Si-based metal–insulator–semiconductor (MIS) photocathodes for water splitting. Our patterned Ag–Pt alloyed catalyst on planar p-Si gave rise to a high incident-photon-to-current conversion efficiency (IPCE) at wavelengths greater than 600 nm. The high IPCE at the red part of the solar spectrum ($\lambda > 600$ nm) is crucial for a real two-photon device.[14] A smaller 3D Ag–Pt catalyst would reflect less light so that more light gets absorbed in the underlying Si. This leads to a higher IPCE and J_{SC} as predicted from full wave electromagnetic simulations.

Experimental

Chemical reagents and materials

All chemicals were used as received from MERCK. Deionized (DI) water (18.2 MΩ) was used throughout this work. All glassware was cleaned with piranha (1 : 3 H_2O_2 : H_2SO_4) and aqua regia (1 : 3 HNO_3 : HCl). A p-type Si(100) (boron doped, 8–12 Ω cm, 700–790 μm thick) and highly doped n^+-Si(100) (phosphorus doped, 0.001–0.002 Ω cm, 700–750 μm) wafers were purchased from Wafer Biz corporation.

Physical characterization

To observe the surface morphology of the photoelectrode, field-emission scanning electron microscopy (FESEM) was used with a SUPRA 55VP (Carl Zeiss) at a 2 kV accelerating voltage at the National Instrumentation Center for Environmental Management of Seoul National University. A cross-sectional view of the photoelectrode was prepared by focused ion beam SMI3050SE (SII Nanotechnology). To observe the metal catalyst layer, depositing spin-on glass (SOG, ED400A S.C3%, APM) was necessary to minimize any damages and to conserve the porous structure of the metal catalyst layer from the ion beam accelerated by high voltage. The SOG was spin-coated on the 3D-patterned Ag–Pt/p-Si(100) photocathode at 500 and 1500 rpm for 5 and 20 s, respectively. In other cases, a gold and carbon layer was used as a protection layer. High-resolution TEM (HRTEM), high-angle annular dark field-scanning TEM (HAADF-STEM), and energy dispersive X-ray spectroscopy (EDS) images were acquired by a JEM-300F (JEOL) at 300 kV at the Research Institute of Advanced Materials (Seoul National University).

Photoelectrochemical measurements

The light source for simulating solar light was a 150 W xenon arc lamp equipped with an air mass filter (1.5 Global). The light intensity was controlled by adjusting the distance from the light source and was calibrated using a radiometer (Solar light, PMA-2100) and a pyranometer (Solar light, PMA-2144). IPCE was measured using a 300 W xenon arc lamp combined with a monochromator. The home-built light source setup was provided by Uninanotech. For the photoelectrochemical measurements, the homemade electrochemical cell with flat, quartz window light transmission was used. Pt wire (AFCTR5, Pine research) and Ag/AgCl (3 M NaCl, Bioanalytical System, Inc.) were used as the counter and reference electrodes, respectively. The Pt wire exposed to electrolyte solution for the hydrogen evolution reaction (HER) was separated with an isolation tube and glass

frits to prevent cross-contamination between H_2 and O_2 gas. The 0.5 M H_2SO_4 solution was purged with high purity (99.999%) H_2 gas for 30 min before conducting voltammetry experiments. The electrochemical measurements started only when the fluctuation of the open circuit potential became within 1 mV range. The potential was converted to RHE potentials by measuring the open circuit potential between the Ag/AgCl electrode *vs.* commercialized RHE (ALS, Japan) in H_2-purged 0.5 M H_2SO_4 solution. The potential sweep rate was 10 mV s^{-1}. For the durability tests, −0.2 V (*vs.* RHE) was applied for 24 h under simulated AM 1.5 illumination. The Faradaic efficiency was calculated by: $2n_{H_2}F/Q$, where n_{H_2} is the total amount of produced hydrogen gas (mol) measured by gas chromatography (GC) (YL6100GC, Young Lin), F is the Faraday constant, and Q is the total amount of charge (C) passed as measured by integrating the current flow for 1 h. The evolved H_2 was collected from headspace of the cell with a known volume, purged with N_2 gas (99.9%). For linear sweep voltammetry under chopped light illumination, an optical chopper (Stanford Research Systems) was employed at 1.5 Hz.

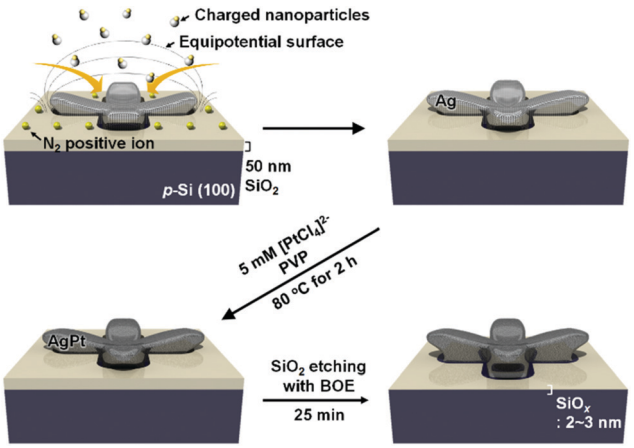

Fig. 1 The preparation scheme of 3D patterned Ag–Pt catalyst on planar p-Si(100).

Results and discussion

Fig. 1 schematically illustrates the fabrication procedure of the 3D-patterned Ag–Pt/p-Si(100) photocathodes for HER. The 3D Ag structures composed of nanoparticles were directly patterned using a multi-pin spark discharge generator (MSDG) and an ion-induced electrostatic focusing method under 25 °C and 1 atm, uniquely developed by Choi's research group.[19] Briefly, we employed a planar p-Si(100) substrate with a cross-patterned 50 nm-thick SiO_2 layer. Then, high voltage was applied to the multi pins and the Si substrate. The generated multi-spark discharge produced charged Ag nanoparticles and ions. The nanoparticles are migrated to the oppositely charged Si substrate by the electrostatic force and the flow of N_2 carrier gas. By an electrostatic lens effect, the charged Ag nanoparticles are assembled at the center of the cross-patterned SiO_x-etched area and grown as 3D flower-shaped structures. The details of the MSDG design are described in our previous studies and in the Experimental section in the ESI.† To introduce more efficient reaction sites for HER, Pt was incorporated by reaction with the pre-patterned Ag structures and $[PtCl_4]^{2-}$ ions at 80 °C through a galvanic exchange reaction. The overall morphology of the catalyst structures was retained through this exchange process, as confirmed by the FESEM images (Fig. S1, ESI†). Finally, the 50 nm-thick SiO_2 layer, playing the role of a mask for the 3D patterning, was etched away by dipping in buffered oxide etch (BOE) solutions. The optimal reaction time with Pt ions and BOE was 2 h and 25 min, respectively. The removal of the 50 nm-thick bare SiO_2 layer is essential for photocurrent generation and will be discussed in detail afterward.

The FESEM images of the 3D-patterned Ag–Pt/p-Si(100) are shown in Fig. 2a and b. The nanoparticles were only deposited at the cross-patterned SiO_2-etched area and grew into four-leaf-clover-shaped structures (Fig. 2a). Fig. 2b shows the magnified image of a single flower-like structure marked by the white dotted rectangle in Fig. 2a. Even after the treatment with BOE, the cross-pattern of the 50 nm-thick SiO_2 layer could still be observed,

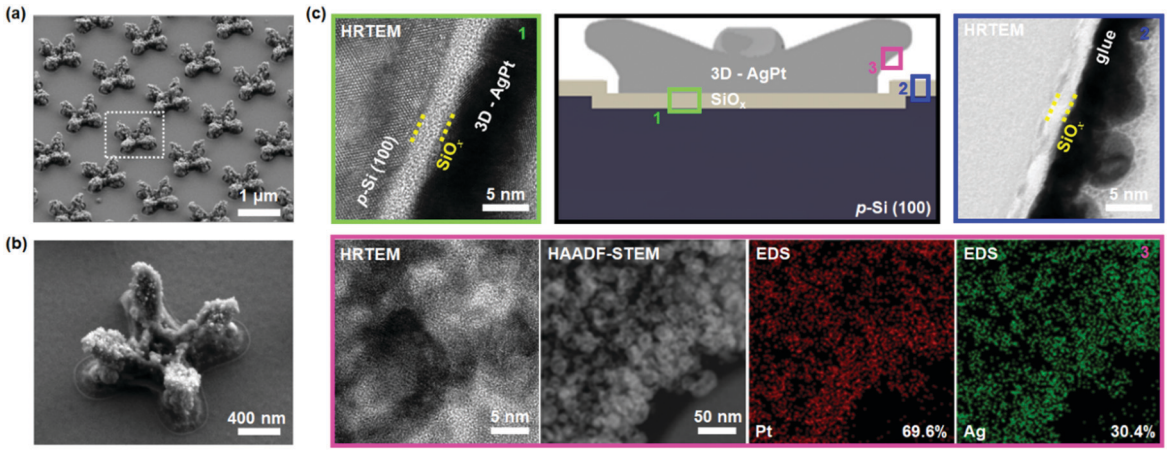

Fig. 2 (a) Tilted FESEM image of the 3D-patterned Ag–Pt/p-Si(100) photocathode. (b) Magnified image of one catalyst structure as shown in the white dotted box in (a). (c) Cross-sectional HRTEM images of each part of our photocathodes. The selected area is marked by the schematic photoelectrode structure with the same color and number.

as shown in the FESEM image (Fig. 2b). For more detailed structural information, we investigated each part of the photoelectrode using cross-sectional high-resolution transmission electron microscopy (HRTEM; Fig. 2c). The regions marked by a number and a colored box in the illustration of the photoelectrode (black dotted box in Fig. 2c) were observed by HRTEM. It was found that a 20 nm deep groove was formed at the Si substrate (Fig. S2, ESI†); this is the region not covered by the artificially deposited SiO_2 layer after generating cross-like pre-patterns using the reactive ion etch process (RIE). Even after the RIE procedure, a native oxide layer of SiO_x existed, and the 3D-patterned Ag structures were deposited on SiO_x/p-Si(100) (green line in Fig. 2c). A SiO_x layer of a similar thickness (2–3 nm) was also observed in the region between the patterned metal structure, which was previously protected by the 50 nm-thick SiO_2 layer (blue box in Fig. 2c). The pre-patterned Ag structures consisted of agglomerated nanoparticles (Fig. S3, ESI†), and this morphology was unchanged after the Pt incorporation step by exchange with 5 mM $[PtCl_4]^{2-}$ through a galvanic replacement reaction (HRTEM and HAADF-STEM images in the pink box). After 2 h of exchange reaction, 70% of Pt was homogeneously incorporated into the 3D-patterned catalyst structure (Fig. 2c). The Pt and Ag as obtained by inductively coupled plasma mass spectrometry (ICP-MS) were 25.72 (±1.89) and 11.18 (±0.0318) μg cm^{-2}.

To examine the effects of the Pt/Ag ratio in the catalyst and SiO_x layer on the photoelectrochemical performance, linear sweep voltammograms were acquired in H_2-saturated 0.5 M H_2SO_4 under AM 1.5 illumination while varying the duration of the Pt exchange reaction and the dipping time in BOE (Fig. 3). The results of this experiment will endow us with an intuitive understanding of how the photogenerated electrons are transferred under photoelectrochemical environments. As a well-known material exhibiting the best electrochemical kinetics for HER in acid solutions, Pt needs to be incorporated for a higher photocurrent density.[17,20] As shown in Fig. 3a, however, the optimal photocurrent density was observed at the atomic Pt/Ag ratio of 2.3 in the 3D-patterned Ag–Pt catalyst. An exchange reaction for longer than 2 h resulted in the incorporation of excessive amounts of Pt (Pt/Ag = 4) in the catalyst structure, thereby deteriorating the performance. This result indirectly corroborated the importance of Ag for the extraction of electrons from p-Si(100). As shown in previous reports, Pt directly attached on SiO_x-covered Si surface is not superlatively suitable for the extraction of photogenerated electrons because of its high work function (ϕ_{Pt}: 5.65 eV[18]), which brings about unfavorable band alignment for minority carrier transfer from Si to Pt through tunneling.[15] The Ti layer beneath the Pt catalyst assists the extraction of photogenerated electrons from p-Si(100) through SiO_2 by tunneling, owing to its lower work function than Pt (ϕ_{Ti}: 4.33 eV[18]), resulting in an enhanced performance.[15] The V_{OC} is sensitive to the difference between the work function of the metal and that of the semiconductor; a larger difference leads to a higher V_{OC} unless there are significant interfacial states, causing more probable carrier recombination.[15,21] Silver is the well-known element that has a comparable work function

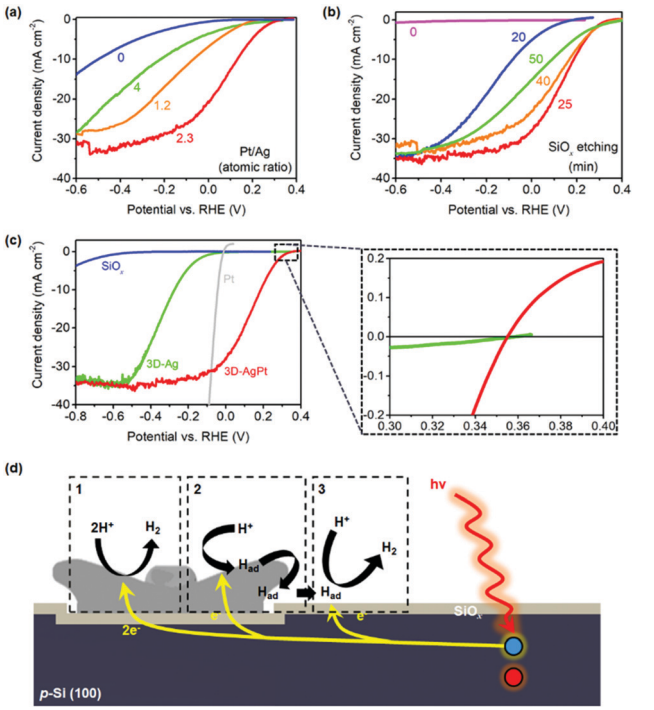

Fig. 3 Linear sweep voltammograms for various (a) atomic Pt/Ag ratios of the patterned catalysts by controlling the duration time for the galvanic exchange reaction of pre-patterned 3D-Ag catalysts with $[PtCl_4]^{2-}$ and (b) BOE etching time. (a) The BOE was treated for 30 min and (b) the reaction time for galvanic replacement was 2 h, respectively. (c) Photoelectrochemical linear sweep voltammograms for HER at the optimized 3D-patterned Ag–Pt/p-Si(100). The voltammograms for 3D-Ag (green line), without the catalyst (blue line), and Pt (gray line) are shown for comparison (left). The voltammograms at Pt were measured by using a Pt rotating disk electrode under the electrode rotation of 1200 rpm. Magnified linear sweep voltammograms from the right panel of Fig. 3c (dotted box) for clear V_{OC} verification (right). For the photoelectrochemical measurements, the electrolyte was H_2-purged 0.5 M H_2SO_4 and the electrode was irradiated by a simulated AM 1.5 illumination (100 mW cm^{-2}). Exposed electrode area was 0.13 cm^2 and the scan rate was 10 mV s^{-1}. (d) Schematic illustration of how HER occurs on our photocathodes.

with Ti and thus forms a Schottky contact with moderately doped Si.[22] To support the effectiveness of Ag as a good interfacial layer for Si-based photocathodes, we patterned a simple dot-shaped Pt/Ag catalyst (diameter/spacing: 50/50 μm) on planar p-Si(100) by varying the Ag thickness (5 *vs.* 30 nm). For a constant Pt thickness (20 nm), the Pt (20 nm)/Ag (30 nm) catalyst pattern gave better voltammograms than 5 nm Ag in the photoelectrochemical measurements in H_2-purged 0.5 M H_2SO_4 (Fig. S4b, ESI†). This better current–voltage curve at thicker Ag (30 nm) was also observed at the solid-state measurements of one dot pattern of Pt/Ag deposited on p-Si(100) under dark conditions. Additionally, the current response at Pt (20 nm)/Ag (30 nm) showed better diode behavior than with the 5 nm layer of Ag (Fig. S4c, ESI†). Thus, it was important to optimize the ratio of Pt/Ag by balancing the reaction kinetics and thermodynamic properties for electron transfer by tunneling. Indeed, a certain amount of Ag underneath the Pt is advantageous for extracting a minority carrier.

As shown in Fig. 3b, the removal of the 50 nm-thick SiO_2 layer, employed as a mask for Ag patterning, is critical to the photoelectrochemical performance of 3D-patterned Ag–Pt/p-Si(100) cathodes. The photocurrent density (-0.12 mA cm^{-2} at 0 V *vs.* RHE) was negligible in the presence of the 50 nm-thick SiO_2 layer, whereas the photocurrent increased significantly (-28 mA cm^{-2} at 0 V *vs.* RHE) after dipping in BOE solutions for 25 min. The photoelectrode performance decreased again, however, under a longer SiO_x etching duration (40 min). The undercut of the SiO_x layer supporting the patterned structure weakened the catalyst adhesion, which may have caused delamination from the substrate, as confirmed by the FESEM analysis (Fig. S5, ESI†). This result indicated that, in addition to the production of H_2 at the patterned Ag–Pt catalysts, the thin insulating layer beneath the patterned catalysts critically affects the generation of the photocurrent density. The current density ratio before and after the removal of 50 nm-thick SiO_2 was surprisingly high (230 calculated as 28/0.12 mA cm^{-2} at 0 V *vs.* RHE), where the coverage factor of the catalyst pattern standing on the 2–3 nm SiO_x layer was around 11%. According to the previous report by Esposito *et al.*,[23] a bare silicon oxide layer not only acts as a protection layer and window for sufficient light absorption, but also participates in the (photo)electrochemical reactions. The SiO_x layer could become conductive and provide additional charge-carrier transport pathways.[23] In addition, it possibly becomes the reaction site for further electron transfer to reduce H_{ad} that spills over from the Pt catalyst for the evolution of H_2 gas[15,23] and/or first electron transfer to generate adsorbed H_{ad} atoms ($H^+ + e^- \rightarrow H_{ad}$).[24] By etching away the thick SiO_2 layer, the thin oxide layer contributes to these processes even more actively.

In general, the HER is a two-electron transfer reaction involving one intermediate, H_{ad}, and may take place through either the Volmer–Heyrovsky or the Volmer–Tafel reaction mechanism:[17]

$$\text{Volmer step: } H^+ + e^- \rightarrow H_{ad} \quad (1)$$

$$\text{Heyrovsky step: } H_{ad} + H^+ + e^- \rightarrow H_2 \quad (2)$$

$$\text{Tafel step: } 2H_{ad} \rightarrow H_2 \quad (3)$$

For deeper insights into the mechanism of HER at the 3D-patterned Ag–Pt catalyst/p-Si(100), we obtained linear sweep voltammograms at various conditions after 2 h and 25 min treatments with $[PtCl_4]^{2-}$ and BOE, respectively, as shown in Fig. 3c. The catalyst pattern composed of only Ag (green line) generated a photocurrent density to a certain extent, while a much lower photocurrent density was observed when the metallic catalyst layer did not exist (blue line). Although the onset potential (V_{onset}, V (*vs.* RHE) for $J = -1.0$ mA cm^{-2}) for 3D Ag/p-Si(100) was 400 mV more negative than for the Ag–Pt catalyst layer (red line), both of their V_{OC} values were nearly identical at 0.36 V (right panel of Fig. 3c in the dotted box and Fig. S6, ESI†). The comparable V_{OC} for Ag and Ag–Pt is in line with the conclusion that Ag is helpful for the extraction of electrons. After the Pt was introduced into the 3D-patterned Ag catalyst structures, the voltammetric behavior was largely improved, especially at the positive potential region. Based on these results, the HER active catalyst should be effective for the spillover of H_{ad} to the SiO_x layer (reaction scheme (2) in Fig. 3d), as well as the direct two-electron transfer for H_2 gas evolution (reaction scheme (1) in Fig. 3d). Conversely, the one-electron electron transfer for proton discharge ($H^+ + e^- \rightarrow H_{ad}$) and H_2 generation (reaction scheme (3) in Fig. 3d) was sluggish at both the bare SiO_x/p-Si(100) and the photocathode substrate with only Ag. The low electrocatalytic activity for HER at the 3D Ag/p-Si(100) was confirmed by the voltammograms of the Ag and Ag–Pt pattern on n^+-Si(100) in Fig. S7 (ESI†). The contribution of bare SiO_x to the photoelectrochemical current, alongside the patterned Pt-based catalysts, is also consistent with previous reports.[15,23,24] The voltammogram obtained under chopped illumination was well-matched with the voltammogram under constant illumination, without any current spikes, indicating facile electron transfer without recombination (Fig. S8, ESI†).[25] A durability test was conducted at -0.2 V (*vs.* RHE) for 24 h under simulated AM 1.5 illumination. The photocurrent density was gradually degraded for the first 2 h, but the stability was maintained afterwards (Fig. S9a, ESI†). It was thought that the initial reduction of the photocurrent was due to the further oxidation of the native SiO_x layer, which is vulnerable when exposed to aqueous electrolyte environments.[26] When comparing the linear sweep voltammograms acquired before and after the durability test, we could observe a slightly lowered photocurrent density after the amperometric experiment while maintaining the initial V_{OC} and V_{onset}. This confirmed that the slight performance reduction comes from the degradation of the insulating layer, not from the Pt losses (Fig. S9b, ESI†).[27] The Faradaic efficiency was 98.6% ($\pm$0.83%) as measured by a gas chromatography instrument under -0.2 V (*vs.* RHE) and AM 1.5 illumination.

We could achieve the near maximum J_{SC} for p-Si as -36 mA cm^{-2} owing to the fact that 89% of the bare SiO_x/Si surface was exposed to the transparent electrolyte solutions for efficient light penetration. However, the V_{OC} of 0.36 V (*vs.* RHE) was *ca.* 100 mV higher than our expectation when considering that our p-Si(100) was covered with the native oxide, which was a low quality tunneling oxide with a large number of defect sites. We next calculated the diode quality factor to evaluate the junction property of the 3D Ag–Pt/p-Si(100). The diode quality factor (n) was determined based on the light-intensity-dependent photovoltage (V_{Ph}) (Fig. 4a) and J_{SC} values using eqn (4),[28]

$$\ln J_{SC} = (q/nkT)V_{Ph} + \ln J_S \quad (4)$$

which was derived using the diode equation, $J = J_S(\exp[q(V - JR_SA)]/nkT - 1) - J_{SC}$, where, q is the charge of an electron (1.60×10^{-19} C), k is Boltzmann's constant (1.38×10^{-23} J K^{-1}), T is the temperature (298 K), J_S is the dark saturation current density (A cm^{-2}), R_S is the series resistance, and A is the electrode area (cm^2). V_{Ph} was determined by the difference in V_{OC} between 3D Ag–Pt/p-Si(100) and 3D Ag–Pt/n^+-Si(100), measured under light and dark conditions, respectively, and the current density in eqn (4) is expressed in units of A cm^{-2}. The n and J_S values, extracted from the slope and y-intercept of

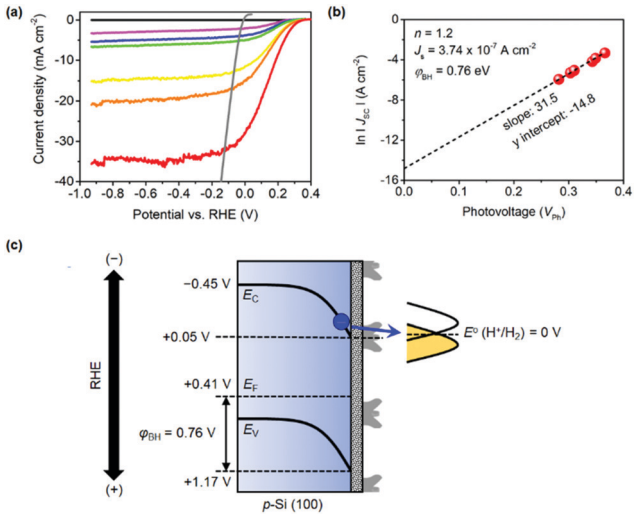

Fig. 4 (a) Linear sweep voltammograms in H_2-purged 0.5 M H_2SO_4 for 3D Ag–Pt/p-Si(100) under various light intensities (red, orange, yellow, green, blue, pink, and black line: 100, 59, 43, 18, 15, 8, 0 mW cm^{-2}). The gray line is for 3D Ag–Pt/n$^+$-Si(100) measured under dark conditions (scan rate: 10 mV s^{-1}). (b) ln(current density)–photovoltage plots calculated from the voltammetry measurements (a) at different light intensities. (c) Schematic band diagram of 3D Ag–Pt/p-Si(100).

the relation between ln J_{SC} and V_{Ph} (eqn (4)), were 1.2 and 3.7 × 10^{-7} A cm^{-2}, respectively (Fig. 4b). Since n was close to 1, the junction was thought to act as a Schottky diode that enables facile extraction of the photogenerated minority carriers, resulting in a high V_{OC} and steep increase in the initial current density.[29] The reported n value for planar p-Si covered with electroless-deposited Pt nanoparticles was 1.3.[29]

Considering the SiO_x, which is not a high-quality oxide layer, as a tunneling barrier on planar Si, these quantitative values reflected in the V_{OC}, J_{SC}, and n values were a fair bit higher than our expectation. As suggested earlier, the synergistic effect of Ag and Pt is a probable reason. Because the Ag and Pt elements are homogeneously distributed in the nanoparticles, we roughly estimated the work function of our Ag–Pt catalyst as 5.2 eV by using the relation of the work function with the atomic proportion, $\phi_{Ag_{30}Pt_{70}} = 0.3 \times \phi_{Ag}(4.26\ eV) + 0.7 \times \phi_{Pt}(5.65\ eV)$.[30] The formation of an alloy of Pt with Ag deflates the high work function of the Pt. This approach enables the improved MIS junction by reducing the voltage drops across the insulating SiO_x layer.[28,31] From the J_S value calculated herein (3.7 × 10^{-7} A cm^{-2}), it is possible to infer the barrier height (φ_{BH}) by using eqn (5) related with the solid-state Schottky diode,[28]

$$\varphi_{BH} = (kT/q)\ln[(A \times T^2)/J_S] \quad (5)$$

where A^* is the effective Richardson's constant (32 A cm^{-2} K^{-2} for p-Si).[32] The barrier height for 3D Ag–Pt/p-Si(100) has been measured to be 0.76 eV. The estimated work function of our Ag–Pt catalyst layer was about 1.0 eV higher than the pure Ag, which was previously measured at a Ag/p-Si(100) Schottky junction in vacuum.[22] It is reasonable that the lowering work function of the catalyst at photocathodes is somewhat effective for the improvement of the barrier height. With the calculated barrier height herein, we could estimate the location of the conduction band edge potential, as shown in Fig. 4c. It could be expected that we would acquire a good performance in spite of the low-quality oxide owing to the large φ_{BH} and well-aligned band edge potentials with protons. In addition, our observation implies that additional factors exist for further enhancement. While the reason is unclear yet, the 'pinch-off' effect might be responsible for this observation. Our patterned catalyst consisted of the homogeneously dispersed alloyed nanoparticles, which provide for the non-uniform barrier height contacts to be smaller than the depletion width of p-Si (2 μm). This inhomogeneous contact can incur anomalous barrier heights that lead to an increased barrier height for both the solid-state and PEC device.[28] Furthermore, we cannot rule out the 3D catalyst structure, which enables a sufficient loading of Pt while minimizing the parasitic interruption of light absorption to Si for the better performance of our photocathodes. Based on the previous report, 20 μg cm^{-2} of Pt loading, deposited by a simple (electro)chemical method, reduced the J_{SC} by −30 mA cm^{-2} because of the inefficient utilization of incoming light by scattering at the Pt catalyst.[23] In our case, the current density was quite high as the photocurrent density at 0 V (*vs.* RHE) and the J_{SC} were *ca.* −28 and −36 mA cm^{-2}, respectively, while maintaining the high V_{OC} for planar p-Si(100). We believe that the high photocurrent density under the high catalyst loading comes from the 3D structures, which enable a low coverage factor for light absorption while ensuring the sufficient amount of catalysts.

We investigated the *J*–*V* curves for photoelectrochemical HER (Fig. 5a) and obtained the incident photon-to-current conversion efficiency (IPCE) (Fig. 5b) by varying the size of the catalyst. A bigger catalyst could be achieved by simply increasing the nanoparticle deposition time, while keeping the other experimental

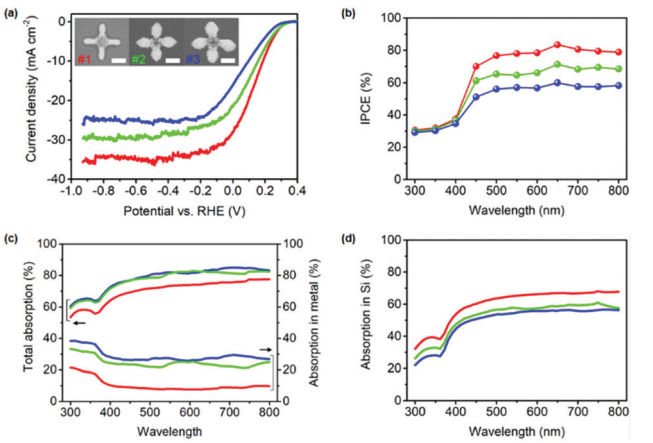

Fig. 5 (a) Linear sweep voltammograms (10 mV s^{-1}) under AM 1.5 illumination at different sizes of the 3D Ag–Pt catalysts patterned on the planar p-Si substrate. The SEM images in the inset show the top-view of the catalyst structure (red line: #1, green line: #2, and blue line: #3). (b) IPCE measured using monochromatic light illumination from a Xe arc lamp under applied bias at −0.4 V (*vs.* RHE). For the photoelectrochemical measurements, all the electrolyte was H_2-purged 0.5 M H_2SO_4. (c) Calculated total absorption and absorption in the metal structure and (d) absorption in the silicon substrate.

conditions constant (see ESI†). As the catalysts grew to become #3, the saturated photocurrent density was reduced by 30% (J_{SC} = −36 mA cm^{-2} at #1 → −25 mA cm^{-2} at #3). This tendency is well reflected in the IPCE results (Fig. 5b), as the opaque catalysts located in the middle of the light path to the semiconductor largely influence the photocurrent generation.

To further verify the interaction between the light and 3D Ag–Pt catalysts, we analyzed the optical properties of the catalysts of different sizes by performing full-wave electromagnetic simulations using the finite difference time domain method. The geometry of the 3D nanostructures was modelled by using the SEM images of the actual structures as illustrated in Fig. S1 and S10 (ESI†), while the dielectric function of Ag–Pt alloy was estimated by using the weighted average method[33,34] and the results were plotted in Fig. S11 (ESI†). Since the structures had a four-fold rotational symmetry, they were insensitive to the polarization of light for normal incidence. Consequently, here we calculated the overall light absorption in the entire device, the absorption in the Ag–Pt catalyst structures, and the absorption in the Si substrate. Fig. 5c shows that the overall absorption in the devices had an opposite tendency to the IPCE measurements; whereby the devices with larger Ag–Pt structures showed a higher total absorption. The benefit from the overall absorption was outweighed by the loss due to absorption in the metal catalyst, which was eventually wasted as heat. Consequently, the smallest structure showed the highest absorption in the Si substrate, which could actually participate in the hydrogen production processes by generating the photogenerated minority carriers. Assuming the internal quantum efficiency of the device was near unity, the absorption in the Si substrate could be directly translated into IPCE, and indeed the theoretically obtained Si absorption (Fig. 5d) and the measured IPCE (Fig. 5b) agree well.

The electromagnetic field profiles further revealed the origin of the different absorption behaviors of the three Ag–Pt catalyst structures (Fig. 6). At a short wavelength regime (<350 nm), the absorption in metallic structures is roughly proportional to their area coverage. For example, at 300 nm wavelength, the metal absorption in structures #1, #2, and #3 were 21%, 33%, and 38%, respectively, which are similar to the ratio of their cross-sectional areas 11 : 17 : 21. As shown in Fig. 6a, d, and g, the electric field intensity profiles do not exhibit any sign of surface mode formation at the wavelength of 300 nm. On the other hand, the absorption in the Ag–Pt catalyst at longer wavelengths was no longer simply proportional to the surface area, but significantly affected by surface plasmon resonances. At the wavelength of 595 nm, the electric fields formed multiple hotspots with similar intensities at the surface of structures #2 (Fig. 6e) and #3 (Fig. 6h), whereas structure #1 did not support a strong surface mode (Fig. 6b). As a result, the absorptions in metal for structures #2 and #3 were 25%, which was more than 3 times higher than that of structure #1. The number and the intensity of plasmonic hotspots depend on the wavelength. At 720 nm, structure #2 had a fewer number of plasmonic hotspots compared to structure #3, as shown in Fig. 6f and i, leading to a 26% lower absorption in metal. Note that, in our device, most of the plasmonic hotspots were formed outside the active layer and

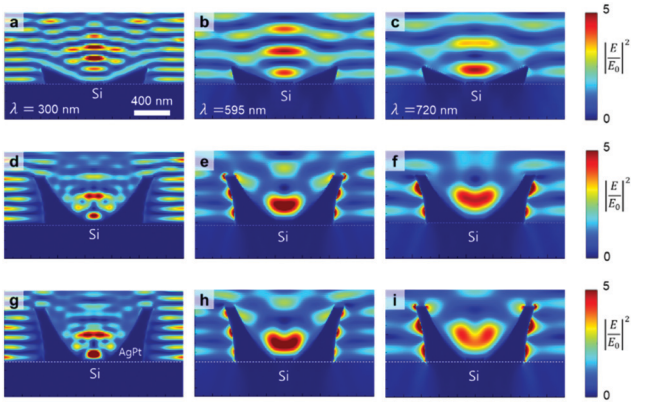

Fig. 6 Electric field intensity profile of structures #1, #2, and #3 for various wavelengths. (a–c) E-field intensity for structure #1 at various wavelengths (lambda, λ) of 300 nm, 595 nm, 720 nm. (d–f) The same for structure #2 and (g–i) the same for structure #3.

therefore could not directly contribute to generating electron–hole pairs for HER processes. By comparing the polarization curve at 3D Ag–Pt/n$^+$-Si(100) measured under the chopped illumination and dark condition, the well-overlapped voltammograms confirmed that the Ag–Pt catalyst pattern itself could not produce charge carriers, leading to additional photocurrent density by hot-electron transfer (Fig. S12, ESI†).[35]

The results from the optical simulations herein are contradictory to our initial expectations that the 3D flower-like catalyst layer consists of nanoparticles that play the roles of not only formulating an advantageous band profile for electron extraction, but also for enhancing the light absorption. Still, it cannot be ruled out that the nanoflower structure helps with the generation of more excitons above 400 nm wavelength, possibly due to a forward scattering enhancement, which could transfer the scattered light to Si.[36,37] However, this does not seem a considerable factor. The high J_{SC} might be largely dependent on the electronic properties at the MIS interface, not from the structure for plasmonic effects. What we have learned from this work is that Pt is much more absorptive than Ag throughout the visible spectrum, and thus the Pt-based catalyst structures are more prone to parasitic absorption loss;[38] therefore, the entire catalyst structure of the PEC system should be carefully designed to minimize the loss of light absorption in the underlying Si layer while sophisticatedly tuning the energetics at the MIS interface.[39] From a structural perspective, our alloyed 3D catalyst pattern could contain a large number of active sites for carrier extraction and transfer while suppressing the light loss by scattering and/or reflection. Further research regarding the structural effects on photoelectrochemical performance are underway in our lab to understand the meaning of this absorption discrepancy acquired through simulation with regard to the photoelectrochemical performance.

Conclusions

In summary, this study described an enhanced photoelectrochemical HER performance at a 3D Ag–Pt catalyst patterned on

planar p-Si(100) and investigated the origins of the improvement in the electronic properties of the MIS junction interface and the optical properties of the flower-like catalyst. By alloying Pt, the most active element for HER, with Ag in the form of agglomerated nanoparticles, the improved activity originated largely from the increased photogenerated minority carrier extraction from Si to the catalyst layer, which arises from the advantageous downward band profile. In part, our patterned catalyst could alleviate the parasitic light loss at the catalyst layer owing to the patterned structure that had a bare Si surface for light penetration together with a sufficient loading of Pt for HER. Not only the formation of anomalous Schottky contacts for the increased barrier height, but also the Ag–Pt alloyed nanoparticles could contribute to a synergistic effect that possibly supplied more H_{ad} from Ag for further reaction at Pt and some spillover to the bare SiO_x layer. In this way, we could simultaneously acquire a V_{OC} of 0.36 V, while retaining a J_{SC} of -36 mA cm^{-2}, which are near the maximum photocurrent density for planar p-Si(100). In addition, the results in this study imply that slightly more dopants with a higher work function of p-Si could possibly improve the semiconductor/electrolyte interface for the photocathode. To date, photoelectrochemical research on 3D catalysts has been relatively less common than on semiconductor structuring to increase the light absorption,[39,40] and there are a number of questions yet to be answered, and thus subsequent studies are needed, *e.g.*, further investigations on the effects of the various coverage factors and overall morphology for further optimization of our photoelectrode. Nevertheless, it is true that the apartment-like catalyst pattern composed of alloyed nanoparticles, which could efficiently manage the charge carrier, light, and the population of the catalyst elements, enables an enhanced photoelectrochemical performance. We expect that this strategy will be applied to non-precious metal catalyst-based solar-fuels generation, which suffers from more severe light loss at the catalysts layer, stemming from the large loading utilization to compensate the insufficient catalytic activity.

Conflicts of interest

There are no conflicts to declare.

Acknowledgements

This work was supported by the Creative Materials Discovery Program (2016M3D1A1900038) (H. H. and M. S. J.), the Global Frontier R&D Program on Center for Multiscale Energy Systems (2012M3A6A7054855) (K. H. and M. C.), and the National Research Foundation of Korea (NRF) grant (2017R1E1A1A01074236) (S. Y. L. and T. D. C.), which are funded by the NRF under Ministry of Science and ICT, Korea.

References

1 M. G. Walter, E. L. Warren, J. R. McKone, S. W. Boettcher, Q. X. Mi, E. A. Santori and N. S. Lewis, *Chem. Rev.*, 2010, **110**, 6446–6473.
2 S. Ardo, D. F. Rivas, M. A. Modestino, V. S. Greiving, F. F. Abdi, E. A. Llado, V. Artero, K. Ayers, C. Battaglia, J. P. Becker, D. Bederak, A. Berger, F. Buda, E. Chinello, B. Dam, V. Di Palma, T. Edvinsson, K. Fujii, H. Gardeniers, H. Geerlings, S. M. H. Hashemi, S. Haussener, F. Houle, J. Huskens, B. D. James, K. Konrad, A. Kudo, P. P. Kunturu, D. Lohse, B. Mei, E. L. Miller, G. F. Moore, J. Muller, K. L. Orchard, T. E. Rosser, F. H. Saadi, J. W. Schuttauf, B. Seger, S. W. Sheehan, W. A. Smith, J. Spurgeon, M. H. Tang, R. van de Krol, P. C. K. Vesborg and P. Westerik, *Energy Environ. Sci.*, 2018, **11**, 2768–2783.
3 Z. G. Zhu, T. K. Tam, F. F. Sun, C. You and Y. H. P. Zhang, *Nat. Commun.*, 2014, **5**, 3026.
4 A. Sarkar and R. Banerjee, *Int. J. Hydrogen Energy*, 2005, **30**, 867–877.
5 B. A. Pinaud, J. D. Benck, L. C. Seitz, A. J. Forman, Z. B. Chen, T. G. Deutsch, B. D. James, K. N. Baum, G. N. Baum, S. Ardo, H. L. Wang, E. Miller and T. F. Jaramillo, *Energy Environ. Sci.*, 2013, **6**, 1983–2002.
6 C. R. Jiang, S. J. A. Moniz, A. Q. Wang, T. Zhang and J. W. Tang, *Chem. Soc. Rev.*, 2017, **46**, 4645–4660.
7 Y. K. Chen, K. Sun, H. Audesirk, C. X. Xiang and N. S. Lewis, *Energy Environ. Sci.*, 2015, **8**, 1736–1747.
8 S. Y. Lim, Y. R. Kim, K. Ha, J. K. Lee, J. G. Lee, W. Jang, J. Y. Lee, J. H. Bae and T. D. Chung, *Energy Environ. Sci.*, 2015, **8**, 3654–3662.
9 M. R. Nellist, F. A. L. Laskowski, F. D. Lin, T. J. Mills and S. W. Boettcher, *Acc. Chem. Res.*, 2016, **49**, 733–740.
10 K. Sun, I. A. Moreno-Hernandez, W. C. Schmidt, X. H. Zhou, J. C. Crompton, R. Liu, F. H. Saadi, Y. K. Chen, K. M. Papadantonakis and N. S. Lewis, *Energy Environ. Sci.*, 2017, **10**, 987–1002.
11 S. Oh, H. Song and J. Oh, *Nano Lett.*, 2017, **17**, 5416–5422.
12 L. Ji, M. D. McDaniel, S. J. Wang, A. B. Posadas, X. H. Li, H. Y. Huang, J. C. Lee, A. A. Demkov, A. J. Bard, J. G. Ekerdt and E. T. Yu, *Nat. Nanotechnol.*, 2015, **10**, 84–90.
13 S. Hu, M. R. Shaner, J. A. Beardslee, M. Lichterman, B. S. Brunschwig and N. S. Lewis, *Science*, 2014, **344**, 1005–1009.
14 B. Seger, T. Pedersen, A. B. Laursen, P. C. K. Vesborg, O. Hansen and I. Chorkendorff, *J. Am. Chem. Soc.*, 2013, **135**, 1057–1064.
15 D. V. Esposito, I. Levin, T. P. Moffat and A. A. Talin, *Nat. Mater.*, 2013, **12**, 562–568.
16 Y. I. Kim, E. Samuel, B. Joshi, M. W. Kim, T. G. Kim, M. T. Swihart and S. S. Yoon, *Chem. Eng. J.*, 2018, **353**, 189–196.
17 Z. W. Seh, J. Kibsgaard, C. F. Dickens, I. B. Chorkendorff, J. K. Norskov and T. F. Jaramillo, *Science*, 2017, **355**, eaad4998.
18 H. B. Michaelson, *J. Appl. Phys.*, 1977, **48**, 4729–4733.
19 H. Kim, J. Kim, H. J. Yang, J. Suh, T. Kim, B. W. Han, S. Kim, D. S. Kim, P. V. Pikhitsa and M. Choi, *Nat. Nanotechnol.*, 2006, **1**, 117–121.
20 C. C. L. McCrory, S. Jung, I. M. Ferrer, S. M. Chatman, J. C. Peters and T. F. Jaramillo, *J. Am. Chem. Soc.*, 2015, **137**, 4347–4357.

21 A. G. Scheuermann, J. P. Lawrence, K. W. Kemp, T. Ito, A. Walsh, C. E. D. Chidsey, P. K. Hurley and P. C. McIntyre, *Nat. Mater.*, 2016, **15**, 99–105.
22 S. Acar, S. Karadeniz, N. Tugluoglu, A. B. Selcuk and M. Kasap, *Appl. Surf. Sci.*, 2004, **233**, 373–381.
23 N. Y. Labrador, X. X. Li, Y. K. Liu, H. Y. Tan, R. Y. Wang, J. T. Koberstein, T. P. Moffat and D. V. Esposito, *Nano Lett.*, 2016, **16**, 6452–6459.
24 S. Y. Lim, D. Han, Y. R. Kim and T. D. Chung, *ACS Appl. Mater. Interfaces*, 2017, **9**, 23698–23706.
25 H. C. Ye, H. S. Park, V. A. Akhavan, B. W. Goodfellow, M. G. Panthani, B. A. Korgel and A. J. Bard, *J. Phys. Chem. C*, 2011, **115**, 234–240.
26 I. Oh, J. Kye and S. Hwang, *Nano Lett.*, 2012, **12**, 298–302.
27 P. C. Dai, J. Xie, M. T. Mayer, X. G. Yang, J. H. Zhan and D. W. Wang, *Angew. Chem., Int. Ed.*, 2013, **52**, 11119–11123.
28 J. C. Hill, A. T. Landers and J. A. Switzer, *Nat. Mater.*, 2015, **14**, 1150–1155.
29 S. W. Boettcher, E. L. Warren, M. C. Putnam, E. A. Santori, D. Turner-Evans, M. D. Kelzenberg, M. G. Walter, J. R. McKone, B. S. Brunschwig, H. A. Atwater and N. S. Lewis, *J. Am. Chem. Soc.*, 2011, **133**, 1216–1219.
30 M. Akbi, A. Bouchou and M. Ferhat-Taleb, *Vacuum*, 2014, **101**, 257–266.
31 I. A. Digdaya, G. W. P. Adhyaksa, B. J. Trzesniewski, E. C. Garnett and W. A. Smith, *Nat. Commun.*, 2017, **8**, 15968.
32 V. W. L. Chin, J. W. V. Storey and M. A. Green, *J. Appl. Phys.*, 1990, **68**, 4127–4132.
33 N. E. Motl, E. Ewusi-Annan, I. T. Sines, L. Jensen and R. E. Schaak, *J. Phys. Chem. C*, 2010, **114**, 19263–19269.
34 S. W. Verbruggen, M. Keulemans, J. A. Martens and S. Lenaerts, *J. Phys. Chem. C*, 2013, **117**, 19142–19145.
35 H. Robatjazi, S. M. Bahauddin, C. Doiron and I. Thomann, *Nano Lett.*, 2015, **15**, 6155–6161.
36 H. A. Atwater and A. Polman, *Nat. Mater.*, 2010, **9**, 205–213.
37 K. R. Catchpole and A. Polman, *Appl. Phys. Lett.*, 2008, **93**, 191113.
38 E. D. Palik, *Handbook of Optical Constants of Solids*, Academic Press, New York, 1997.
39 W. Vijselaar, P. Westerik, J. Veerbeek, R. M. Tiggelaar, E. Berenschot, N. R. Tas, H. Gardeniers and J. Huskens, *Nat. Energy*, 2018, **3**, 185–192.
40 R. Xu, L. Y. Wen, Z. J. Wang, H. P. Zhao, S. P. Xu, Y. Mi, Y. Xu, M. Sommerfeld, Y. G. Fang and Y. Lei, *ACS Nano*, 2017, **11**, 7382–7389.

